Giant dipole resonance in neutron-rich nuclei within the phonon damping model

Nguyen Dinh Dang,[1,*] Toshio Suzuki,[2] and Akito Arima[3]
[1]*RI-beam Factory Project Office, The Institute of Physical and Chemical Research, 2-1 Hirosawa, Wako City, Saitama 351-01, Japan*
[2]*Department of Physics, College of Humanities and Sciences, Nihon University, Sakurajosui 3-25-40, Setagaya-ku, Tokyo 156-8550, Japan*
[3]*House of Councillors, Nagata-cho 2-1-1, Chiyoda-ku, Tokyo 100-8962, Japan*
(Received 19 October 1999; published 8 May 2000)

The damping of the giant dipole resonance (GDR) in neutron-rich nuclei ^{18,24}O, ^{60}Ca, and ^{150}Sn is calculated within the phonon damping model (PDM) and compared with those in β-stable isotopes. The Hartree-Fock single-particle energies obtained employing the SGII interaction are used in calculations. The PDM parameter for the ph-phonon interaction between the levels close to the Fermi surface in exotic nuclei has been chosen to simulate the strong coupling between the GDR phonon and dense incoherent ph configurations. The results of the calculations show the appearance of a low-lying structure (pigmy resonance) in all exotic nuclei under consideration. The calculations at nonzero temperature show that the GDR in hot medium and heavy neutron-rich nuclei exhibits a similar behavior as those of the hot GDR in stable nuclei. The pigmy resonance is smoothed out with increasing temperature.

PACS number(s): 21.10.Pc, 24.30.Cz, 21.60.−n, 24.10.Pa

I. INTRODUCTION

The prospects of using radioactive beams to explore nuclei far from the β-stability line has sparked intensive experimental and theoretical studies of neutron-rich nuclei during recent years. The presence of the neutron halo [1] leads to the appearance at low excitation energies of a new type of excitation, the soft dipole mode [2], which has been experimentally observed in ^{11}Be [3] and ^{11}Li [4].

When the binding energy approaches zero, coupling to the continuum becomes very important. Large gaps between proton and neutron binding energies in exotic nuclei lead to a big difference in neutron and proton level spacing. As a result, the GDR distribution in exotic nuclei is getting more fragmented. Because of the large spatial separation between the center of mass and the center of charge, low electric dipole oscillations can result and show up at the tail of the usual isovector giant dipole resonance (GDR) as what are called pigmy resonances. In oxygen isotopes [5–7] the pigmy resonance region is below 17 MeV. Both the soft dipole mode and the pigmy resonance are due to the neutron excess in nuclei. However, the soft dipole mode is a feature of very light (halo) systems such as ^{6}He, ^{11}Li, and ^{11}Be, in which the coupling to unbound neutrons in the continuum is crucial. The pigmy resonance, the subject of the present paper, appears in medium and heavy nuclei, where the neutron excess can form the neutron skin. These are some common features of the GDR in exotic nuclei that have been obtained in a number of theoretical calculations within the random phase approximation (RPA) [8,9], relativistic RPA (RRPA) [10], the self-consistent Hartree-Fock plus RPA (HF+RPA) [11], and large scale shell model calculations [12]. In these calculations, the damping of the GDR has not been explicitly calculated, but the strength distributions were just smeared out by a Lorentzian with a finite width. The question of how the damping of the GDR affects the strength of the pigmy resonance in exotic nuclei still remains open.

Recently, the authors of Refs. [13,14] have proposed and developed the phonon damping model (PDM), which describes the damping of the GDR via the coupling of the GDR phonon to incoherent particle-hole (ph) configurations, as well as particle-particle (pp) and hole-hole (hh) ones that appear at nonzero temperature ($T\neq 0$). The PDM is a simple yet microscopic approach that has proven to be quite successful for the description of width and shape of the hot GDR as a function of temperature [13–15]. The PDM has also been extended to the study of the multiphonon resonances, in particular the double and triple GDRs in Refs. [16,17]. Since the properties of the single-particle spectra to which the GDR phonon is coupled within the PDM are crucial for the fine structure of the damped GDR, the presence of the dense unbound neutron single-particle states in neutron-rich nuclei will make the total strength distribution of GDR differ from the one obtained in stable nuclei. The aim of the present work is to test the capability of the PDM in the study of GDR damping in neutron-rich nuclei.

The paper is organized as follows. Section II recapitulates in brief the main feature of the PDM-1 [13], which is necessary for the extension of PDM to the study of GDR in exotic nuclei. The results of numerical calculations of the damping of GDR in ^{18,24}O, ^{60}Ca, and ^{150}Sn will be analyzed and discussed in Sec. III in comparison with those in stable nuclei ^{16}O, ^{40}Ca, and ^{120}Sn. The results of calculations at nonzero temperature $T\neq 0$ are also presented. The paper is summarized in the last section, where some conclusions are drawn.

II. OUTLINE OF THE PDM

The PDM describes the coupling of collective oscillations (phonons) to the field of incoherent nucleon pairs [13,14]

*On leave of absence from the Institute of Nuclear Science and Technique, Hanoi, Vietnam. Electronic address: dang@rikaxp.riken.go.jp

 ©2000 The American Physical Society

making use of a Hamiltonian that is composed of three terms

$$H=\sum_{s} E_s a_s^\dagger a_s+\sum_{q} \omega_q Q_q^\dagger Q_q+\sum_{s,s',q} F_{ss'}^{(q)} a_s^\dagger a_{s'}(Q_q^\dagger+Q_q). \tag{1}$$

The first term on the right-hand side (RHS) of Eq. (1) corresponds to the field of independent single particles, where $a_s^\dagger$ and a_s are the creation and destruction operators of a particle or hole state with energy $E_s=\epsilon_s-\epsilon_F$, ϵ_s the single-particle energy and ϵ_F the chemical potential. The second term is the phonon field, where $Q_q^\dagger$ and Q_q are the creation and destruction operators of a phonon with energy ω_q. The last term describes the coupling between the phonon field and the field of all possible ph, pp, and hh pairs. The indices s and s' denote particle (p, $E_p>0$) or hole (h, $E_h<0$), while the index q is reserved for the phonon state $q=\{\lambda,i\}$ with multipolarity λ (the projection μ of λ in the phonon index is omitted for simplicity). In general, the sums in the last two terms are carried out over $\lambda\geqslant 1$. The coupling vertex $F_{ss'}^{(q)}$ is parametrized for the GDR ($\lambda=1$) within the PDM-1 as $F_{ph}^{(1)}=F_1$ and $F_{pp'}^{(1)}=F_{hh'}^{(1)}=F_2$, whose selection for use with the Hartree-Fock single-particle spectra will be discussed in Sec. III. The form of the Hamiltonian (1) is quite common in many microscopic models to nuclear collective excitations. The difference between models is in the definition of the single-particle energy E_s, phonon energy ω_q, and phonon structure using a specific effective coupling $F_{ss'}^{(q)}$. In a fully microscopic picture, the structure of phonon operators $Q_q^\dagger$ and Q_q can be defined as a superposition of collective ph pairs such as in RPA.

The main equations of the PDM-1 for the damping of the GDR phonon due to coupling to the incoherent ph, pp, and hh configurations by means of the Hamiltonian (1) have been derived in Ref. [13] making use of the double-time Green function method [19]. The equation for the propagation of the GDR phonon is

$$G_q(E)=\frac{1}{2\pi}\frac{1}{E-\omega_q-P_q(E)}, \tag{2}$$

where $P_q(E)$ is the polarization operator

$$P_q(E)=\sum_{ss'} F_{ss'}^{(q)}F_{s's}^{(q)}\frac{n_s-n_{s'}}{E-E_{s'}+E_s}. \tag{3}$$

The function n_s is the single-particle occupation number, which can be well approximated by a Fermi-Dirac distribution function at temperature T. The imaginary part of the analytic continuation of the polarization operator into the complex energy plane $P_q(\omega\pm\varepsilon)$ (ω real) yields the damping $\gamma_q(\omega)$ of the GDR phonon

$$\gamma_q(\omega)=\pi\sum_{ss'} F_{ss'}^{(q)}F_{s's}^{(q)}(n_s-n_{s'})\delta(\omega-E_{s'}+E_s). \tag{4}$$

The full width at the half maximum (FWHM) of the GDR is calculated as

$$\Gamma_{\rm GDR}=2\gamma_{q={\rm GDR}}(\omega=E_{\rm GDR}), \tag{5}$$

where $E_{\rm GDR}$ is the GDR energy. We refer to Ref. [13] for the detailed derivation of these equations.

The strength function of the GDR is calculated as [13–15]

$$S(E_\gamma)=\frac{1}{\pi}\frac{\gamma_{\rm GDR}(E_\gamma)}{(E_\gamma-E_{\rm GDR})^2+[\gamma_{\rm GDR}(E_\gamma)]^2}, \tag{6}$$

where the GDR energy $E_{\rm GDR}$ is defined as the pole of the Green function $G_q(E)$ (2), i.e., as the solution of the equation

$$E_{\rm GDR}-\omega_{\rm GDR}-P_{\rm GDR}(E_{\rm GDR})=0. \tag{7}$$

The moments are calculated from the strength function (6) as

$$m_k=\int_{E_1}^{E_2} S(E)E^k dE, \tag{8}$$

in which the first moment m_1 is the energy weighted sum (EWS) of strengths, which is ultimately related to the Thomas-Reiche-Kuhn (TKR) sum rule of the GDR. The latter is exhausted by integrating the GDR cross section

$$\sigma(E_\gamma)=\frac{4\pi^2e^2\hbar}{mc}\frac{NZ}{A}S(E_\gamma)E_\gamma \tag{9}$$

up to around 40 MeV, namely,

$$\sigma_{\rm int}=\int_0^{40\ {\rm MeV}}\sigma(E_\gamma)dE_\gamma\simeq 60\frac{NZ}{A}({\rm MeV\,mb}). \tag{10}$$

The structure of Eqs. (2) and (3) shows that the GDR strength, which is originally concentrated in an idealized single-phonon state with energy ω_q [Fig. 1(a)], spreads over many ph (at zero and nonzero T) as well as pp and hh (at nonzero T) configurations due to the coupling between the GDR phonon and the background of the incoherent ph, pp, and hh states [Fig. 1(b)]. This is a realization of the common mechanism proposed by Goldhaber and Teller many years ago in Ref. [18], according to which coupling of the ordered dipole vibration to other degrees of freedom broadens the discrete giant dipole states. Many elaborated theoretical models of the damping of giant resonances have studied this mechanism on different microscopic levels. The distribution of the total GDR strength over these states [Fig. 1(c)], therefore, depends on the property of the single-particle spectra from which these configurations are constructed. In the next section, we will see how this makes the damping of GDR in neutron-rich nuclei different from the one in stable nuclei.

III. RESULTS OF NUMERICAL CALCULATIONS

In this section we present the results of calculation for the strength function (6) and EWS of strengths of the GDR in ^{16,18,24}O, ^{40,60}Ca, and ^{120,150}Sn. We employ the same scenario, which has been successfully used to describe the damping of the hot GDR within the PDM-1 [13]. This scenario assumes that, before coupling to the incoherent ph

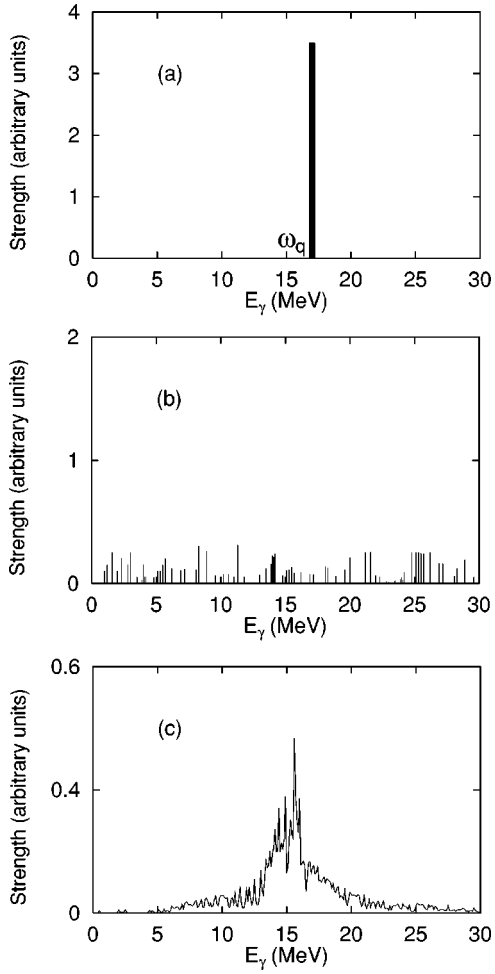

FIG. 1. Illustration of the damping mechanism of the GDR within the PDM. The idealized GDR is generated by the phonon operator $Q_q^\dagger$ with energy ω_q and exhausts all the oscillator strength (a). It is coupled via the last term of the Hamiltonian (1) to the incoherent ph (at zero and nonzero T) and pp and hh (at $T\neq 0$) pairs $a_s^\dagger a_{s'}$ displayed in (b). As a result, the GDR in (a) spreads over many ss' states as depicted in (c).

configurations (as well as pp and hh ones, additionally at nonzero T), all the oscillator strength of the GDR is concentrated in a single collective and structureless phonon with energy ω_q that is close to the observed energy $E_{\rm GDR}^{\rm exp}$ of the GDR built on the ground state (i.e., at $T=0$).

A. Ingredients for numerical calculations

The PDM has been using so far the single-particle energies calculated within the Woods-Saxon potentials. In the present paper, for the application to exotic nuclei, we employ the single-particle energies that have been calculated within the Hartree-Fock (HF) theory using the SGII interaction [20] in the spherical basis. These energies have been used with some success in the study of GDR in exotic nuclei within HF-RPA [8,11]. The validity of the single-particle spectra obtained using different Skyrme-type interactions in the description of neutron-rich nuclei has been discussed in detail in Ref. [21].

TABLE I. The PDM parameters selected using the HF single-particle energies with SGII interaction.

Nucleus	ω_q (MeV)	F_1 (MeV)
^{16}O	22.2	1.025
^{40}Ca	18.4	3.464×10^{-1}
^{120}Sn	16.2	1.732×10^{-1}

Superfluid neutron pairing is not taken into account for simplicity. Its effect on the GDR in stable nuclei is known to be small. In unstable nuclei, the inclusion of pairing may improve the description of the pigmy resonance. The part of spectra that spans the energy region from -60 MeV up to 30 MeV has been used in calculations of the GDR damping.

The phonon energy ω_q and the matrix elements of the coupling to ph and pp or hh, $F_{ph}^{(q)}=F_1$ for $(s,s')=(p,h)$, and $F_{pp}^{(q)}=F_{hh}^{(q)}=F_2$ for $(s,s')=(p,p')$ or (h,h'), are introduced as parameters of the model. Even though the higher-order graphs were not included explicitly in the equations within the PDM-1, this procedure implies that their effects are incorporated effectively in the parameters F_1 and F_2. The PDM-2, which includes this coupling explicitly up to two-phonon terms [14], gives similar results for the hot GDR.

The PDM is not a purely phenomenological model since the GDR energy and width are not input parameters but calculated from microscopic expressions (5) and (7), which contains the PDM parameters. The latter have been determined as follows. The energy ω_q and the parameter F_1 for β-stable nuclei have been chosen so that the GDR width $\Gamma_{\rm GDR}$ calculated from Eq. (5) is equal to the observed FWHM of the GDR, and the GDR energy $E_{\rm GDR}$ calculated from Eq. (7) is equal to the experimentally extracted GDR energy $E_{\rm GDR}^{\rm exp}$. The selected values of the parameters ω_q and F_1 are given in Table I for ^{16}O, ^{40}Ca, and ^{120}Sn making use of the Hartree-Fock single particle spectra mentioned above. The parameter F_2 is chosen so that the GDR energy does not vary appreciably when T changes. This has been achieved with the value of $F_2=40/3F_1$ for all nuclei under consideration.

Since the experimental data for energy and width of GDR in neutron-rich nuclei are not available at present, we extrapolate the values of the parameters determined for a stable nucleus in Table I to its neutron-rich isotopes. With increasing the number of neutrons, the neutron chemical potential $\epsilon_{\rm F}^{\rm N}$ increases from -11.01 MeV in ^{16}O to -4.03 MeV in ^{24}O, from -12.65 MeV in ^{40}Ca to -3.26 MeV in ^{60}Ca, and from -8.46 MeV in ^{120}Sn to -3.1 MeV in ^{150}Sn. In this way, the neutron chemical potential enters the region of dense and weakly bound single-particle levels. This corresponds to the decrease of binding energy of the last neutrons, an effect that leads to a neutron skin. A fully microscopic way of taking into account the effect of small separation energy in nuclear far from stability should treat explicitly coupling to continuum. This goes beyond the scope of the PDM and immediately makes the calculations of configuration mixings become very involved, losing the simplicity

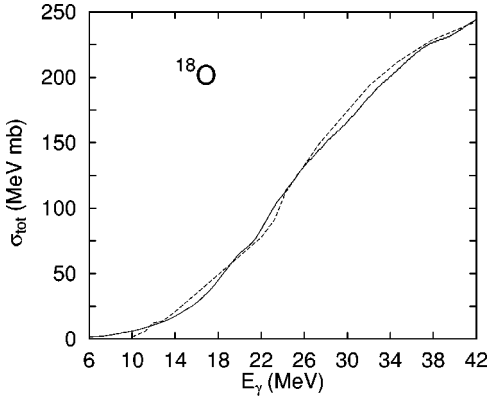

FIG. 2. Running sums of the integrated photoabsorption cross section for ^{18}O. The solid curve is the result of theoretical calculations within the PDM, while the dashed curve is the experimental result of Ref. [1].

and transparentness of the model. Therefore, we prefer to simulate the effect of small separation energy in neutron-rich nuclei by an effective coupling that is simple to handle without increasing the configuration space, which has been used so far for the GDR in stable nuclei within the PDM. The simplest way to realize this in the present calculations is to increase the absolute values of the matrix elements $F_{ph}^{(1)}$ of the coupling between the GDR phonon and the ph configurations that correspond to the neutron levels within a small area near the Fermi surface in neutron rich nuclei. In the present scheme, this corresponds to an increase of parameter F_1 to a value $F_1' \geqslant F_1$ within the region near the neutron Fermi level $\epsilon_F^N \geqslant -8$ MeV, where the difference between the ph-level distance and $|\epsilon_F|$ is not larger than a critical distance $\Delta\epsilon_{crit}$. In order to apply the same large value of F_1' to all the neutron levels within the region defined by the parameter $\Delta\epsilon_{crit}$, the latter must be sufficiently small so that the gross structure of the GDR is not affected. We found that the shape of the main peak of the GDR does not change appreciably with varying $\Delta\epsilon_{crit}$ within the interval 0.5–1.5 MeV. The value $\Delta\epsilon_{crit}=1.5$ MeV has been used in calculations. The value F_1' has been chosen to obtain the best fit to the experimental running sums of the GDR integrated photoabsorption cross section in ^{18}O [5] as displayed in Fig. 2. This gives the value $F_1'=40F_1$. The experimental values of EWS of strengths of GDR in medium and heavy neutron rich nuclei are not available at present. Therefore, we apply the same ratio, obtained in ^{18}O, to the nuclei under consideration. This gives us the value of F_1' equal to 41 MeV for oxygen isotopes, 13.856 MeV for calcium isotopes, and 6.928 MeV for tin isotopes. It is known that the effect of coupling to continuum on the GDR in medium and heavy stable nuclei is less important than the one in lighter nuclei. Therefore, we expect that such kind of extrapolation may provide us with some upper limit for the effect of small separation energy in heavy neutron-rich nuclei under consideration. More experimental data are required in order to refine the value of F_1' depending on the mass number.

We see that the new parameter $\Delta\epsilon_{crit}$ defines the size of the region at the Fermi surface in neutron-rich nuclei where there are excitations of weakly bound ph states [10], which are effectively taken into account by increasing F_1 to F_1' in this region. As will be seen below, this leads to the appearance of the pigmy resonance in neutron-rich nuclei.

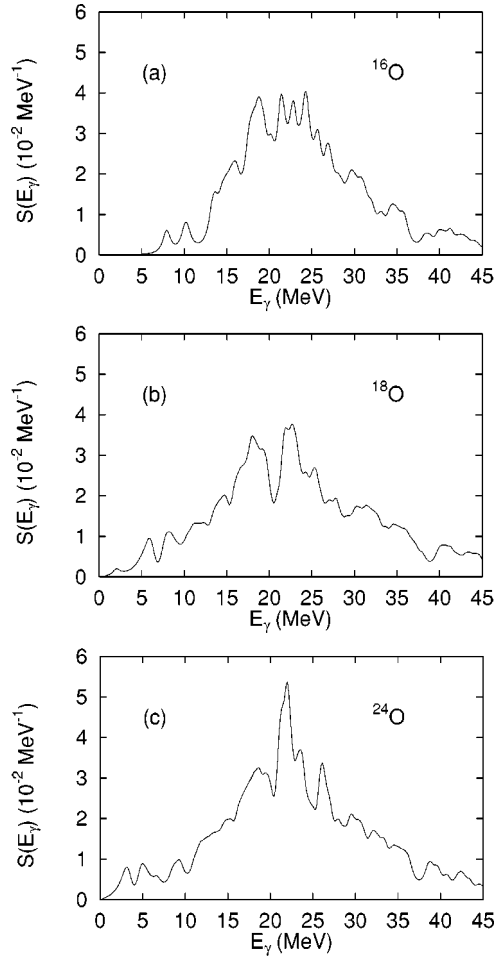

FIG. 3. GDR strength functions in ^{16}O (a), ^{18}O (b), and ^{24}O (c).

It is worth noticing that, since the phonon operator in PDM is considered as boson, it commutes with the ph pair operator. In this sense the Pauli principle is not taken into account mathematically. However, this shortcoming is corrected in practice as long as two parameters ω_q and F_1 are selected to describe correctly the GDR at $T=0$ as discussed above. Therefore, the correction due to Pauli principle and some other effects such as higher-order configuration mixing are effectively included in the parameters of the model.

The calculations also use a value of the smearing parameter ε equal to 0.5 MeV for the analytic continuation of the Green functions to the complex energy plane. This yields the smooth curves for the calculated GDR strength functions. The averaged properties of the GDR such as the width, centroid energy, and the moments are stable against varying ε within 0.1 and 1.0 MeV.

B. Analysis of results obtained

The calculated strength functions of the GDR in oxygen isotopes are shown in Fig. 3. The resonance region in ^{16}O [Fig. 3(a)] is in between 20–25 MeV in agreement with the

TABLE II. The values of the first moment m_1 of GDR m_1^L in the low-energy region ($0 \leqslant E_\gamma \leqslant 10$ MeV), m_1^H in the high-energy region ($10 < E_\gamma \leqslant 40$ MeV), and the fraction $m_1^L/m_1^{\rm tot}$ of the total moment m_1 covered by the low-energy region.

Nucleus	m_1^L	m_1^H	$m_1^L/m_1^{\rm tot}$ (%)
^{16}O	0.12	13.6	0.86
^{18}O	0.34	13.1	2.6
^{24}O	0.33	14.7	2.2
^{40}Ca	0.06	17.8	0.3
^{60}Ca	0.27	18.0	1.5
^{120}Sn	0.26	14.2	1.8
^{150}Sn	0.70	14.1	4.7

experimental observation [22]. The centroid energy of the GDR distribution is located at $E_{\rm GDR} = 22.5$ MeV. The fragmentation of the GDR is rather broad and several distinct peaks can be seen in the resonance region. The GDR strength functions in neutron-rich isotopes ^{18}O and ^{24}O have a tail that is extended toward very low excitation energy, where several small peaks can be seen below 10 MeV and exhaust 2.6 and 2.2% of the total EWS of the GDR strengths, respectively (Table II). This is about 2.6–3.0 times larger than the fraction of the total EWS of strengths within the same energy region in ^{16}O. The centroid energies $E_{\rm GDR}$ of the GDR in ^{18}O and ^{24}O are 22.5 and 22.9 MeV, respectively, i.e., almost at the same place as the GDR in ^{16}O. In ^{18}O, the four major peaks below 15 MeV located at around $E_\gamma = 6$, 8, 11, and 15 MeV can be compared with the four peaks between 7 and 15 MeV observed in experiments [5–7]. The GDR itself has two major peaks located at around 17.5 and 24 MeV. These are to be compared with the broad structure between 17–22 MeV and a strong peak at around 24 MeV found in experiments [5]. No experimental data are available at present for the GDR in ^{24}O, where we expect a major peak at 22.5 MeV and a group of pronounced peaks below 10 MeV [Fig. 3(c)].

Figure 4 shows the calculated strength functions of GDR in ^{40,60}Ca and ^{120,150}Sn. All the GDRs are well localized at around 20 and 15.5 MeV for calcium and tin isotopes, respectively. The shape and FWHM of the GDR do not change significantly with increasing the neutron number. The values of the FWHM are around 7.0–7.5 MeV for calcium isotopes, and 4.8–5.0 MeV for tin isotopes. In the region of $E_\gamma < 10$ MeV, a pronounced pigmy resonance is seen in ^{60}Ca and ^{150}Sn. The fraction of the total EWS of strengths covered by the region below 10 MeV is also around 2.6–3 times larger compared to the same region in the corresponding stable nuclei. In ^{150}Sn, the pigmy resonance's region exhausts almost 5% of the total EWS of GDR strengths (Table II). The overall shapes of the GDRs including the pigmy resonance obtained in the present calculations are similar to those obtained within the full-RPA approach in Ref. [9]. In the latter the GDR width was not calculated, but introduced empirically.

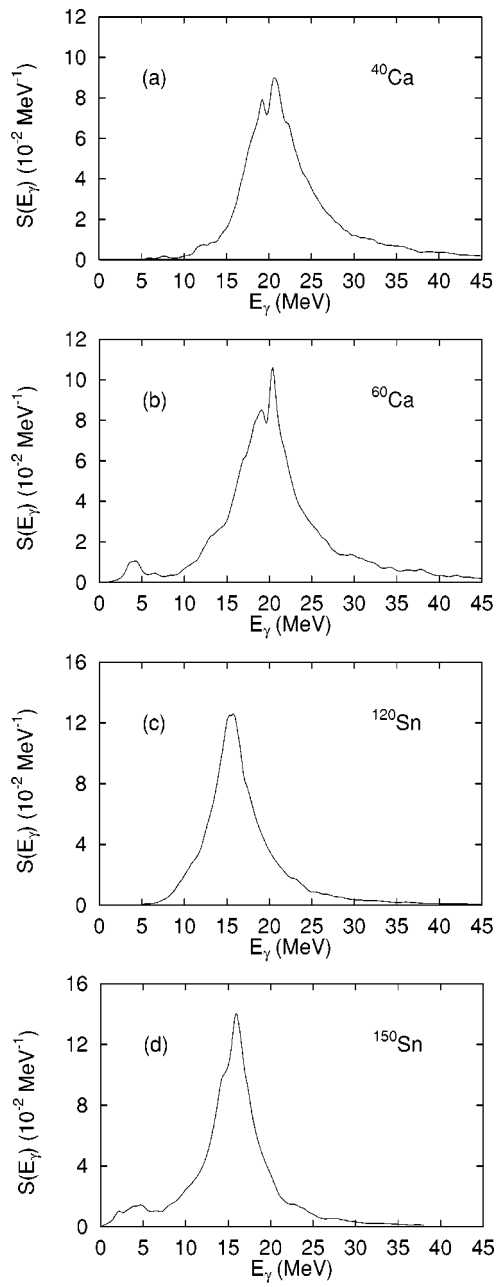

FIG. 4. GDR strength functions in ^{40}Ca (a), ^{60}Ca (b), ^{120}Sn (c), and ^{150}Sn (d).

Shown in Fig. 5 are the GDR strength functions in neutron-rich nuclei ^{60}Ca and ^{150}Sn at several temperatures. The results have been obtained using the values of chemical potentials $\epsilon_{\rm F}^{\rm Z}$ and $\epsilon_{\rm F}^{\rm N}$ that have been determined at $T=0$ [Figs. 5(a) and 5(c)] as well as using the chemical potentials that vary with T to conserve the particle numbers [Figs. 5(b) and 5(d)]. These panels show that the effect of temperature dependence of chemical potentials on the damping property of the GDR in medium and heavy spherical nuclei can be neglected, given the large error bars of available experimental data of hot GDR. The behavior of the hot GDR width as a function of temperature is the same as in stable nuclei [13–15]. The width increases sharply with increasing T up to around 2–3 MeV, but saturates at higher temperatures. Con-

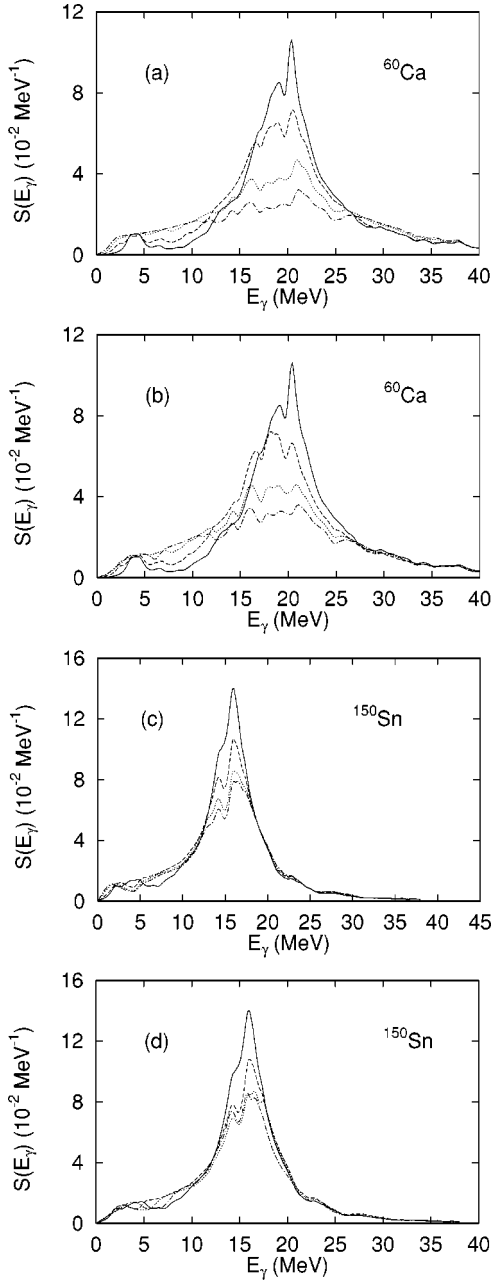

FIG. 5. GDR strength functions in ^{60}Ca (a),(b) and ^{150}Sn (c),(d) at several temperatures. The solid, dashed, dotted, and dash-dotted curves correspond to temperatures $T=0$, 1, 2, and 3 MeV, respectively. (a) and (c): results obtained using the zero-temperature chemical potentials. (b) and (d): results obtained using the temperature-dependent chemical potentials.

cerning the pigmy resonance, it is smoothed out with increasing T. At $T=3$ MeV, no bump structure can be seen below $E_\gamma=10$ MeV, except for a long low-energy tail of the GDR, which should be hard to be extracted from the background of the γ-decay spectra emitted from highly excited nuclei.

IV. CONCLUSIONS

In the present work, we made an attempt to extend the PDM [13,14] to describe the damping of GDR in exotic nuclei. The strength functions of the GDR in neutron-rich nuclei ^{18,24}O, ^{60}Ca, and ^{150}Sn have been calculated within the PDM-1 [13] and compared with the results in the corresponding β-stable nuclei. The results obtained have shown that, given reasonable single-particle spectra (e.g., the HF ones calculated using SGII interaction in the present case), we can determine a unique set of the PDM parameters for each atomic number Z to have a description in agreement with available experimental observations.

The analysis of numerical results allows us to draw the following conclusions.

(i) The appearance of the low-lying GDR (the pigmy resonance) in neutron-rich nuclei can be described within the PDM as a result of a strong coupling of the GDR phonon to the ph configurations in the region around the Fermi surface, where the weakly bound single-particle levels are located close to each other. In the region below 10 MeV, the damped pigmy resonance accounts for up to around 5% of the total EWS of the GDR strengths.

(ii) Except for the low-energy tail of the GDR including the pigmy resonance, the general gross structure of the GDR in neutron-rich nuclei, especially in ^{60}Ca and ^{150}Sn, including the energy, FWHM, and overall shape, is similar to the one in β-stable nuclei.

(iii) The GDR in neutron-rich nuclei at nonzero temperature exhibits the same behavior as the one in stable nuclei. Its width increases sharply with increasing temperature up to around 3 MeV, and saturates at higher temperatures. The centroid energy of the GDR remains nearly temperature independent. The pigmy resonance, however, is smoothed out with increasing temperature.

We have considered only neutron-rich nuclei in the present paper. The application to proton-rich nuclei can be carried out in the same manner. The inclusion of neutron pairing can also improve the quantitative description, especially for the low-lying dipole mode.

ACKNOWLEDGMENTS

Numerical calculations were carried out using a 64-bit Alpha AXP workstation running Digital UNIX (OSF/1) at the Computer Science Laboratory of RIKEN.

[1] I. Tanihata *et al.*, Phys. Rev. Lett. **55**, 2676 (1985); I. Tanihata *et al.*, Phys. Lett. **160B**, 380 (1985).
[2] P.G. Hansen and B. Jonson, Europhys. Lett. **4**, 409 (1987).
[3] T. Nakamura *et al.*, Phys. Lett. B **331**, 296 (1994).
[4] D. Sackett *et al.*, Phys. Rev. C **48**, 118 (1993); F. Shimoura *et al.*, Phys. Lett. B **348**, 29 (1995); M. Zinser *et al.*, Nucl. Phys. **A619**, 151 (1997).
[5] J.G. Woodworth, K.G. McNeil, J.W. Jury, R.A. Alvarez, B.L.

Berman, D.D. Faul, and P. Meyer, Phys. Rev. C **19**, 1667 (1979).
[6] T. Aumann *et al.*, Nucl. Phys. **A649**, 297c (1999).
[7] H. Harada, Y. Shigetome, H. Ohgaki, T. Noguchi, and T. Yamazaki, Phys. Rev. Lett. **80**, 33 (1998).
[8] I. Hamamoto, H. Sagawa, and X.Z. Zhang, Phys. Rev. C **57**, R1064 (1998).
[9] P.G. Reinhard, Nucl. Phys. **A649**, 305c (1999).
[10] Z. Ma, H. Toki, B. Chen, and N. Van Giai, Prog. Theor. Phys. **98**, 917 (1997).
[11] F. Catara, E.G. Lanza, M.A. Nagarajan, and A. Vitturi, Nucl. Phys. **A624**, 449 (1997); E.G. Lanza, *ibid.* **A649**, 344c (1999).
[12] H. Sagawa and T. Suzuki, Phys. Rev. C **59**, 3116 (1999); T. Suzuki, H. Sagawa, and P.F. Bortignon, Nucl. Phys. **A662**, 282 (2000).
[13] N. Dinh Dang and A. Arima, Phys. Rev. Lett. **80**, 4145 (1998); Nucl. Phys. **A636**, 427 (1998).
[14] N. Dinh Dang, K. Tanabe, and A. Arima, Phys. Rev. C **58**, 3374 (1998); Phys. Lett. B **445**, 1 (1998); Nucl. Phys. **A645**, 536 (1999).
[15] N. Dinh Dang, K. Eisenman, J. Seitz, and M. Thoennessen, Phys. Rev. C **61**, 027302 (2000).
[16] N. Dinh Dang, K. Tanabe, and A. Arima, Phys. Rev. C **59**, 3128 (1999).
[17] N. Dinh Dang, K. Tanabe, and A. Arima, Nucl. Phys. A (to be published).
[18] M. Goldhaber and E. Teller, Phys. Rev. **74**, 1046 (1948).
[19] N.N. Bogolyubov and S. Tyablikov, Sov. Phys. Dokl. **4**, 6 (1959); D.N. Zubarev, Sov. Phys. Usp. **3**, 320 (1960); *Non-equilibrium Statistical Thermodynamics* (Plenum, New York, 1974).
[20] N. Van Giai and H. Sagawa, Nucl. Phys. **A371**, 1 (1981).
[21] I. Hamamoto, H. Sagawa, and X.Z. Zhang, Phys. Rev. C **53**, 765 (1996).
[22] J.T. Caldwell, R.L. Bramblett, B.L. Berman, R.R. Harvey, and S.C. Fultz, Phys. Rev. Lett. **15**, 976 (1965).